JOURNAL OF APPLIED ELECTROCHEMISTRY **29**: 229–238, 1999.


# Characterization of porous aluminium oxide films from a.c. impedance measurements

J. A. GONZÁLEZ, V. LÓPEZ, A. BAUTISTA, E. OTERO

*Centro Nacional de Investigaciones Metalúrgicas, Avda Gregorio del Amo 8, E-28040 Madrid, Spain*

X. R. NÓVOA

*Departamento de Ingeniería Química, ETSII, Universidad de Vigo, Spain*

Received 3 November 1997; accepted in revised form 28 April 1998

An equivalent circuit (EC) that reproduces the a.c. impedance of porous aluminium oxide films in a highly approximate manner is proposed. The results reveal that electrochemical impedance spectroscopy (EIS) is a powerful tool for obtaining detailed information on the electrochemical properties of both the porous and barrier layer on which the corrosion resistance of aluminium depends. The impedance at a given frequency can be used for accurate calculation of the electrochemical parameter for the oxide film represented by each element of the EC. In this way, the effects of any factor on sealing and ageing of anodized aluminium oxide films can be precisely analysed. The EIS technique provides an effective, advantageous alternative to existing seal quality control tests.

Keywords: *ageing*, *aluminium*, *anodizing*, *sealed specimens*, *unsealed specimens*

## 1. Introduction

### 1.1. *Sealing of porous aluminium oxide films*

Aluminium anodizing is most often performed in sulphuric acid solutions, which produce a porous closed-packed array of columnar hexagonal cells each consisting of a central pore 10–25 nm in diameter surrounded by a 10–20 nm thick oxide wall normal to the substrate surface and separated from it by a barrier layer (Fig. 1) [1].

The porous structure of these layers makes them highly absorbent and hence prone to fouling and corrosion in aggressive environments. Many applications of anodized aluminium therefore entail the sealing of pores. Industrially, this has traditionally been accomplished by immersion in boiling de-ionized water, a procedure known as hydrothermal sealing (HTS).

The absorbing capacity of anodized coatings also endows them with many advantages that enable, among other, colouring of the materials for use in a variety of ornamental, architectural and household applications. The increased hardness of aluminium oxide relative to the bare metal protects it from wear, one of its few weaknesses.

The uses of anodized aluminium rely very heavily on its sealing, the quality of which must be strictly controlled. Current seal quality control tests range from the extremely simple dye spot test and fixed frequency admittance measurements to the acid dissolution test [2]. All are inexpensive, expeditious and readily applied at a production line, which makes them highly suitable for quality control purposes. However, they are inadequately sensitive for distinguishing seal quality levels above those established by accepted standards; as a result, deriving precise information on the intricate mechanism of sealing and the transformations that occur in the porous and barrier layer entails using much more sensitive techniques. Electrochemical impedance spectroscopy (EIS) [3–11] and transmission electron microscopy (TEM) have proved highly suitable for this purpose [12–16].

In this work, we assessed the potential of EIS for obtaining information on material changes during sealing of aluminium oxide layers and, particularly, on the ageing process during their service lives, a topic which has scarcely been investigated to date. For comparison purposes, traditional quality control tests and the TEM technique were also employed.

### 1.2. *Characterization of anodized films by EIS*

Between the pioneering work of Hoar and Wood [3] involving an impedance bridge and currently available techniques for measuring frequency responses, a number of authors have used EIS to characterize the barrier and porous layer present in anodized aluminium and its alloys [3–11].

Various equivalent circuits have been proposed to model the response of porous aluminium oxide films under different conditions. Thus, Hoar and Wood suggested the ECs of Fig. 2(a) and (b) to model unsealed and partially sealed anodized films, respectively; in the Figure, $R_{sol}$ denotes the solution resistance, $R_{pw}$ the resistance of the pore walls of the

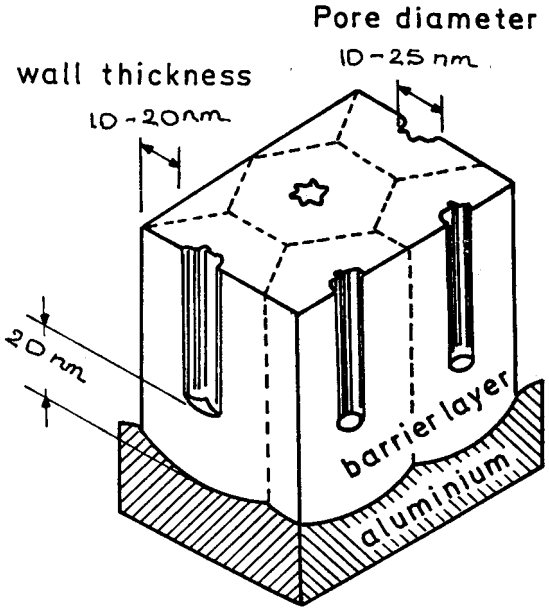


Fig. 1. Schema of the structure of the unsealed oxide layers formed on aluminium.

hexagonal cells in the oxide film, $C_{pw}$ the capacitance in parallel with $R_{pw}$, $R_e$ the resistance of the electrolyte that fills the pores (in parallel with pore walls), and $R_b$ and $C_b$ the resistance and capacitance of the barrier layer. In partially sealed films (Fig. 2(b)), a distinction should be made between the resistance of a very short plug of the pores, $R_{1-1}$, and the associated capacitance, $C_{1-1}$, in series with the resistance and capacity of the remaining pore length ($R_{1-2}$ and $C_{1-2}$, respectively), which will be partly shut up to the barrier layer. Hitzig *et al.* [4, 5] proposed the EC of Fig. 2(c) to account for the behaviour of sealed layers with pits. In the circuit, $\theta$ denotes the fraction of unaltered surface; $(1 - \theta)$ that of pits; $R_p$ and $R_b$ the resistance of the porous and barrier layer, respectively; $R_t$ the charge-transfer resistance of the pits; and $C_p$, $C_b$ and $C_d$ the capacitances associated in parallel to the previous three resistances. (The double layer capacitance, $C_d$, results from the sole contribution of the $(1 - \theta)$ surface fraction.) In films containing no defects $\theta = 1$ and the EC of Fig. 2(c) can be simplified to that of Fig. 2(d).

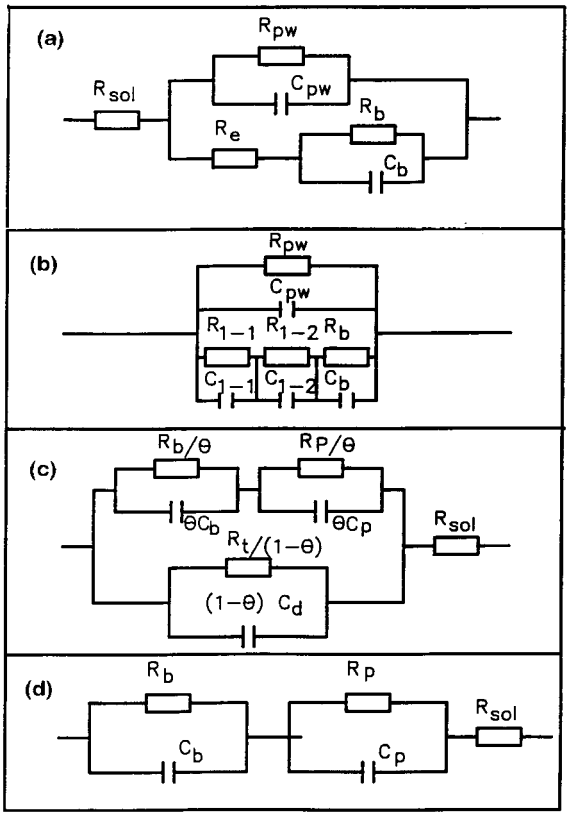


Fig. 2. Selected ECs used for modelling the behaviour of anodized films.

Taking into account that $R_b$ is usually so high that it prevents the passage of current across it, the EC of Fig. 2(d) can be reduced to that of Fig. 3(a) for sealed layers. The new, simplified circuit includes three elements that result in as many straight segments in the impedance diagrams for well-sealed films (Fig. 3(c)), from which the values for such elements can be calculated with enough accuracy for many practical purposes. In unsealed films, pores are filled by the test solution and short-circuit the outer surface and barrier layer; the situation is very approximately reproduced by the oversimplified EC of Fig. 3(b). Figure 3(c) and (d) complement the previous simplified ECs with the experimental impedance diagrams for a properly sealed (45 min in boiling water) and an unsealed anodized specimen. They also illustrate the procedure for estimating roughly electrochemical parameters for anodized films, although the results in this work have been calculated by a procedure of computer fitting, based on a more complex EC proposed later.

## 2. Experimental details

### 2.1. *Material*

The working electrodes used were 5 cm × 10 cm × 0.1 cm plates of 99.5% pure aluminium that were anodized under technical conditions in 18% sulphuric acid at 20 °C and 1.5 A $dm^{-2}$ for 45 min, followed by repeated rinsing and final drying with pressurized air. The oxide films thus obtained were approximately 20 $\mu$m thick.

### 2.2. *Working conditions*

Following anodizing, specimens were subjected to the following treatments: (a) Sealing in boiling de-ionized water for 1, 2, 6, 12, 15, 20 and 45 min. (b) Exposure of specimens, both unsealed and sealed for 45 min, to the urban atmosphere of the University Campus of Madrid for periods from 1 month to 20 years.

### 2.3. *Methods*

Prior to and after atmospheric exposure for 1, 2, 3, 5, 17 and 20 years, impedance diagrams for sealed and unsealed aluminium oxide films were recorded. In

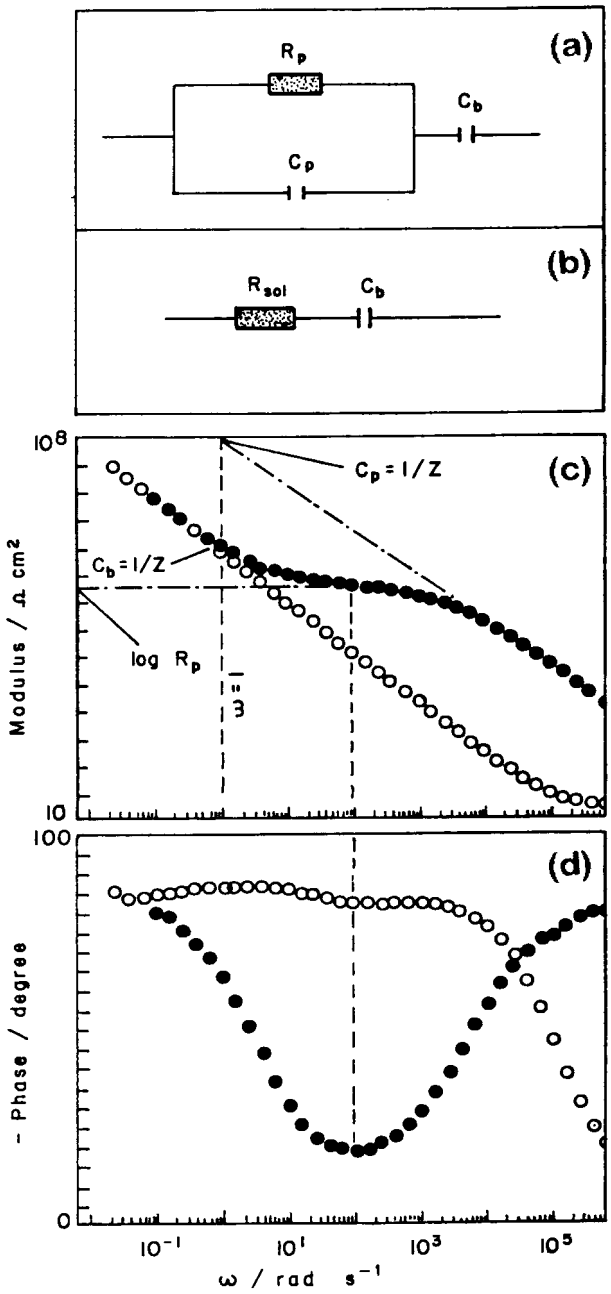


Fig. 3. Simplified ECs (a) and (b), and experimental impedance diagrams for properly sealed (●) and unsealed anodized films (○).

addition, specimens were analysed by using standard tests such as the phosphochromic acid dissolution, dye spot and 1 kHz admittance tests, originally designed for hydrothermally sealed anodized aluminium.

A.c. impedance measurements were made in an unstirred aerated 3.5% (w/w) potassium sulphate solution at 25 ± 1 °C. The surface area exposed to the solution was 1 $cm^2$. The cell and experimental set-up used were described in detail elsewhere [7–10].

Longitudinal sections of anodized films, obtained by pulling and by cutting under a microtome, were examined morphologically under a scanning and a transmission electron microscope, respectively. Ion-beam thinned anodic films were also inspected under the TEM, after their separation from the substrate by dissolution in $HgCl_2$ solution.

## 3. Results

Figure 4(a) shows a cross-sectional view of an anodized film aged for two years in the atmosphere of Madrid. The TEM revealed a structure consisting of parallel bands that resolved into an array of particles of lower density in the zone occupied by the original pores. The walls of hexagonal cells were seen as darker bands. Figure 4(b) shows a conventional transmission electron micrograph of the ion-beam thinned unsealed anodic film prior to exposure. Starting from the diameter of the pores and dimensions of the cells in this micrograph, it is calculated that the transversal section of the pores is about the 17% of the total apparent surface.

As can be seen from the scanning electron micrographs of Fig. 5, during sealing in boiling de-ionized water, an intermediate layer is formed underneath the outer surface that no longer exhibits the band structure, which, however, is still seen (less sharply, however, than in Fig. 4(a)) at a great depth.

Figure 6 shows the impedance diagrams for specimens sealed in boiling de-ionized water for variable lengths of time. Sealing for 45 min was enough to meet the quality standards of traditional control tests. As can be seen, the transformations involved in the sealing process reflect in the medium and high frequency regions (approximately 1–$10^3$ Hz and >$10^3$ Hz, respectively), to which the properties of the porous layer, the only one that undergoes major changes by effect of sealing, are related. In some frequency zones of these ranges, the responses of unsealed and well-sealed anodized films differ by as much as 2–3 orders of magnitude; this makes EIS a highly sensitive technique for assessing seal quality.

Figure 6 displays the rapid changes that take place during industrial sealing; Fig. 7 reflects other essential, slower changes that occur during service life, which have been studied to a much lesser extent to date. Figure 7 compares the impedance diagrams for newly anodized specimens, both sealed in boiling de-ionized water for 45 min (top) and unsealed (bottom), with those for similar specimens that were atmospherically exposed for 1, 5, 17 and 20 years. Atmospheric exposure results in autosealing of unsealed films and resealing of initially sealed films. Thus the modulus of the impedance for the inflexion point portion of the phase angle, which can be used as a quantitative measure of seal quality (Fig. 6), increases by roughly three orders of magnitude throughout the ageing process of porous anodized films, both sealed and unsealed.

## 4. Discussion

### 4.1. *Fitting experimental results to various equivalent circuits*

For practical purposes, the simplified ECs of Fig. 3(a) and (b) will be assumed to approximate accurately enough the behaviour of anodized films in

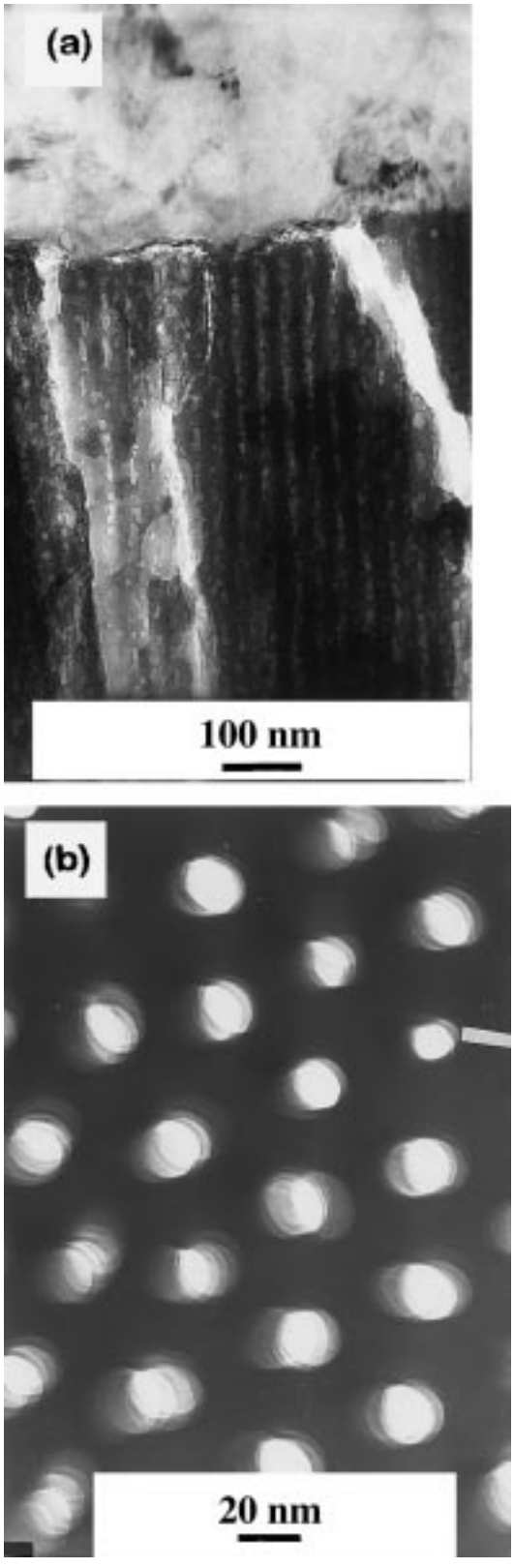


Fig. 4. TEM micrograph of anodized film allowed to autoseal for two years in the atmosphere of Madrid, showing a band structure in the zone near the barrier layer (a), and cross-sectional view of newly anodized unsealed film (b).

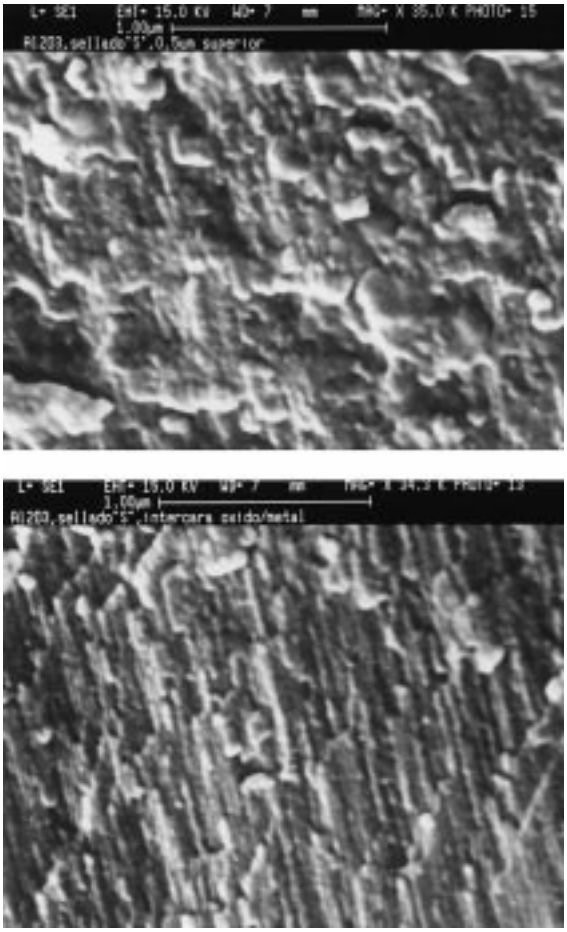

Fig. 5. Scanning electron micrographs of the oxide film/atmosphere interface. In the sealed specimen the formation of an intermediate layer (top) destroys the band structure of the porous layer (bottom).

most situations [4, 5]. Based on our own experience in fitting results by using these simplified ECs [7–10], $C_b$ and $C_p$ for well-sealed films lie in the $\mu F\,cm^{-2}$ and $nF\,cm^{-2}$ range, respectively. As regards resistances, $R_p$ varies from about $10^5\,\Omega\,cm^2$ in 'adequately' sealed specimens (Figs 3(c) and (6)) to values 2–3 orders of magnitude higher, depending on the ageing extent and conditions (Fig. 7) [8, 9], while $R_b$ is so high ($>10^8\,\Omega\ cm^2$) that it cannot be estimated unless the experimental frequency range is extended below 1 mHz, the minimum frequency used in the test (Figs 3, 6 and 7). On the contrary, $R_{sol}$ is usually a few ohms and can only be observed at very high frequencies (close to or above $10^5$ Hz, Fig. 6).

However, the consistency between experimental and calculated through computer fitting values can be improved by using the EC in Fig. 8 instead of the simplified ECs of Fig. 3(a) and (b), the latter two involve fewer electrochemical parameters in the fitting. This is clearly reflected in Figs 9 and 10, which show the fitting of the experimental results for an unsealed anodized specimen aged in the Madrid atmosphere for two years to the ECs of Figs 3(a) and 8, respectively.

Appropriate software allows the computation of the parameter values for the EC of Fig. 8 [17]. Thus, the impedance for the two serial *R*C circuits is given by

$$Z_a = \frac{R_p}{1 + (j\omega R_p C_p)^{\alpha_p}} + \frac{R_b}{(1 + j\omega R_b C_b)^{\alpha_b}} \qquad (1)$$

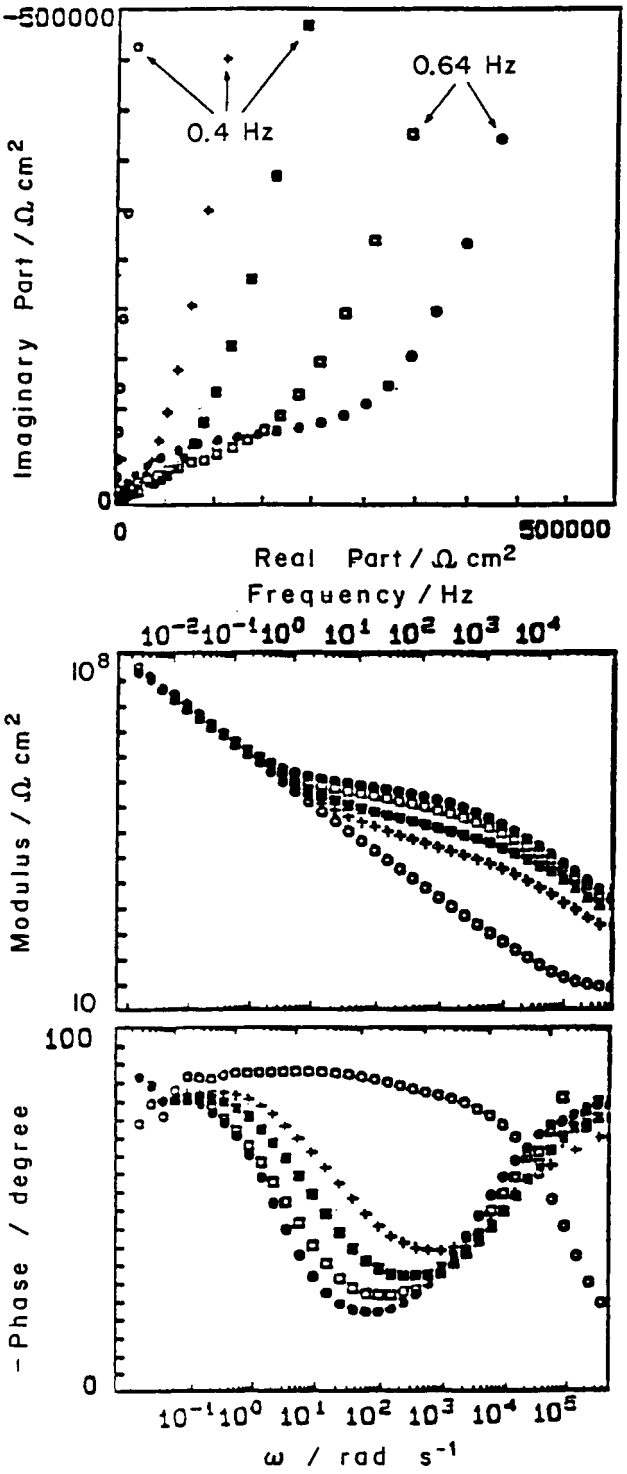


Fig. 6. Variation of impedance with the time of sealing in boiling de-ionized water. (○) Unsealed specimen. Specimens sealed for (+) 2 min, (■) 6 min, (□) 15 min and (●) 45 min.

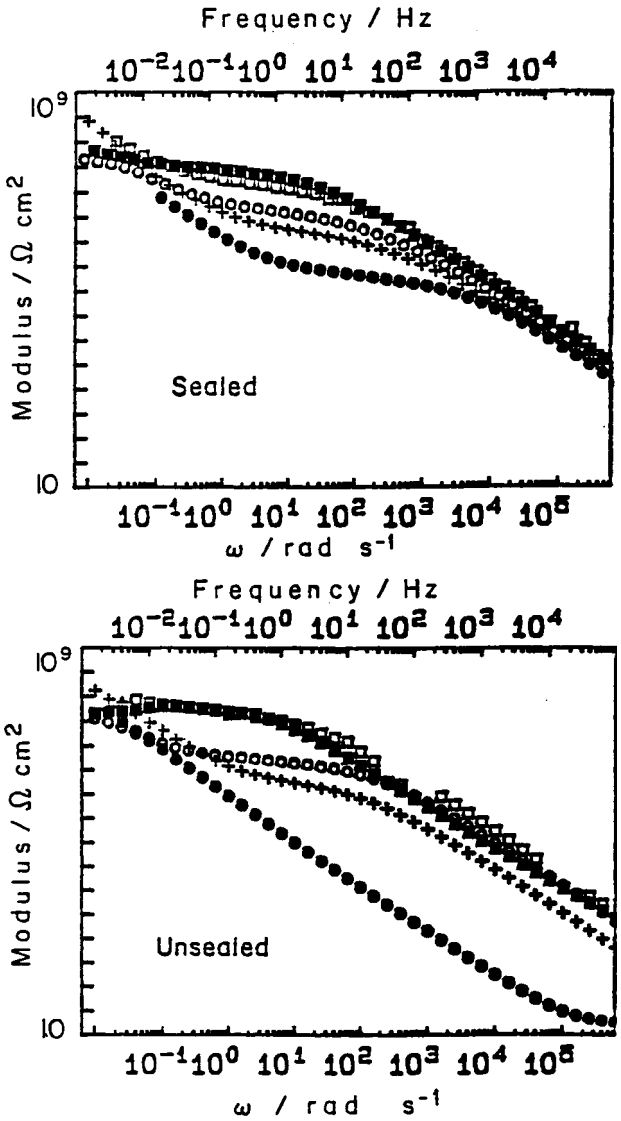


Fig. 7. Bode diagrams for sealed (top) and unsealed specimens (bottom), newly anodized (●), and after (+) 1, (○) 5, (□) 17 and (■) 20 years of atmospheric exposure (ageing).

while the equivalent impedance for the circuit of Fig. 8 can be expressed as

$$Z_t = R_{sol} + \frac{R_1}{(1 + j\omega C_{pw} R_1)^{\alpha_1} + (R_1/Z_a)} \qquad (2)$$

Table 1 gives the parameter values calculated from the data of Fig. 7 for newly sealed specimens and anodized unsealed specimens (the latter aged atmospherically for 0, 1, 2, 3, 17 and 20 years). The tranverse section of the pores, which is about 17% of the total apparent surface (Fig. 4(b)), has been taken into account for the calculation of $C_p$, $R_p$ and $C_{pw}$.

However, the proposed EC can never be a significant advance or a useful source of information in estimating the electrochemical parameters for anodized aluminium oxide films unless all its elements can be assigned physical significance. We use the scheme of Fig. 11, based on reported data [12–16] and on the columnar structure of anodized films shown in Figs 4 and 5, to seek such significance. It can be assumed that the composition of the hexagonal cell walls and barrier layer are the same, namely, anhydrous alumina containing an appreciable proportion of sulphate ions (as $Al_2(SO_4)_3$) from the anodizing bath that will vary little with time. On the other hand, the pore filling, consisting of hydrated alumina (mono-, trihydrate or a mixture of both), changes enormously with the extent of sealing and ageing during atmospheric exposure. Finally, there is an outer layer, referred to as the 'intermediate layer', which is formed by diffusion from the outside very rapidly at boiling

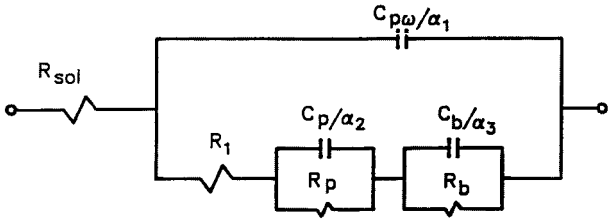


Fig. 8. Proposed EC for sealed anodized films.

temperature at the expense of the columnar structure of the porous layer at the interface with the atmosphere, as shown by the micrographs of Fig. 5. The scheme in the Fig. 11 places each EC component in its appropriate place.

$R_{sol}$ is the resistance of the electrolyte in the test cell; its exact magnitude cannot be ascertained because it can be determined only at frequencies well above 100 kHz. One of the two parallel branches will be formed by the walls of hexagonal cells (with uniform or nearly uniform dielectric properties), represented by $R_{pw}$ and the associated capacitance, $C_{pw}$. The other branch will be formed by the resistance $R_1$ of the electrolyte in the pores and defects of the intermediate layer, in series with pores as a whole (the barrier layer lying at their bases). The electrochemical

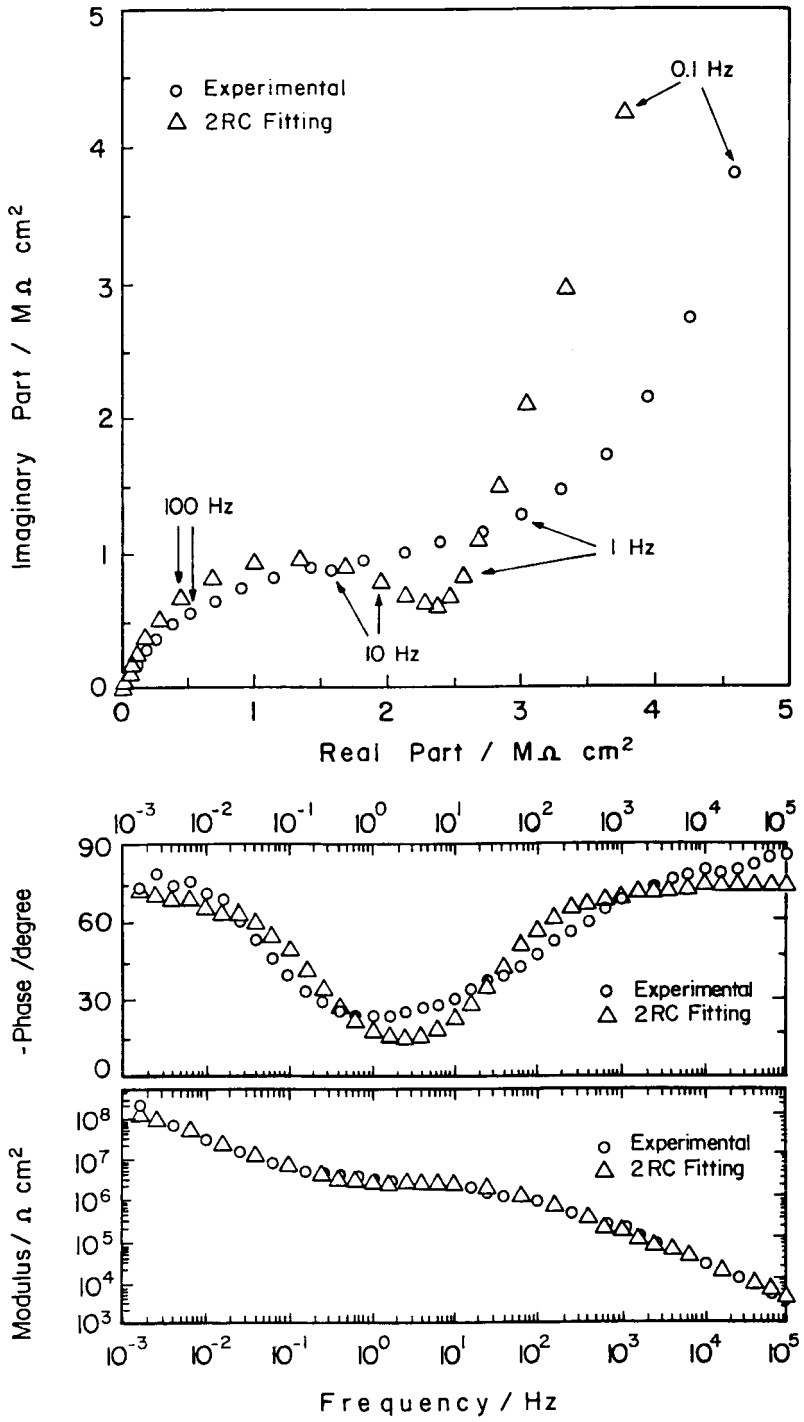


Fig. 9. Nyquist and Bode diagrams showing experimental impedance values (○) for an unsealed anodized specimen after two years of atmospheric ageing. (△) Best fit obtained using the simplified EC of Fig. 3(a). (○) Experimental values.

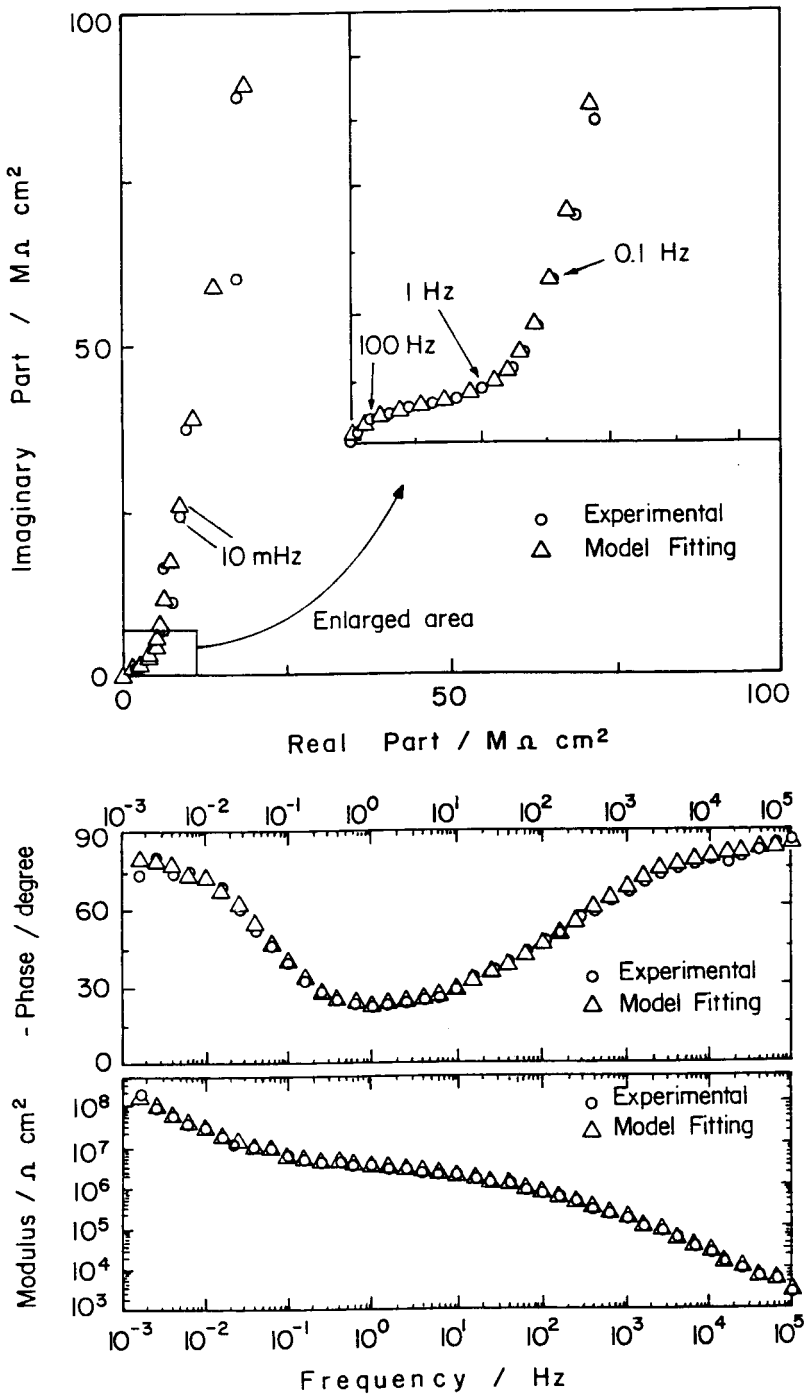


Fig. 10. Nyquist and Bode diagrams showing the fitting of the data in Fig. 9 to the EC of Fig. 8. (○) Experimental values. (△) Fitted values.

properties of the pore filling, $R_p$ and $C_p$, vary dramatically during sealing and/or ageing (exposure), whereas those of the barrier layer, $R_b$ and $C_b$, hardly change. The computational program used permits distinction between $C_{pw}$ and $C_p$, which appear as a single straight segment at high frequencies in impedance diagrams (Figs 3(c), 6 and 7). $C_b$ is about three orders of magnitude greater than $C_{pw}$ or $C_p$, and hence easy to differentiate.

$C_{pw}$ is not reflected in the first branch for unsealed films because it is short circuited by the conducting solution in open pores. Conversely, $R_{pw}$ is very high, so it will never allow the passage of current; as a result, it can be eliminated from the calculations and the EC simplified to that of Fig. 8. This resistance is included in the EC of Fig. 2(b), which was proposed by Hoar and Wood for partially sealed films [3]. In a recent paper, Celati *et al.* [11] used a very similar EC to analyse the behaviour of anodized aluminium films sealed to a variable extent in chromic acid.

### 4.2. *Determination of electrochemical parameters for anodized films*

Parameter $R_1$, which was not considered in previous work, might vary markedly with the extent of sealing

*Table 1. Fitted parameter values*

Column 2 corresponds to specimens subjected to HTS for 45 min and the following columns to unsealed specimens immediately after anodizing (column 3) and after atmospheric exposure for 1, 2, 3, 17 and 20 years (columns 4–8)

| *Parameter* | *Exposure conditions* (*file*) | | | | | | |
|---|---|---|---|---|---|---|---|
| | *S45MIN* | *SS0A* | *SS1A* | *SS2A* | *SS3A* | *SS17A* | *SS20A* |
| $R_{sol}/\Omega\,cm^2$ | 7.4 | 15 | $6.1 \times 10^{-3}$ | $7.0 \times 10^{-4}$ | $2.2 \times 10^{-2}$ | $2.2 \times 10^{-4}$ | 270 |
| $R_1/k\Omega\,cm^2$ | 19.6 | – | 144 | 144 | 41.5 | 267 | 13.8 |
| $C_{pw}/nF\,cm^{-2}$ | 1.8 | – | 5.3 | 0.90 | 1.4 | 0.70 | 0.78 |
| $a_1$ | 0.906 | – | 0.903 | 0.934 | 0.943 | 0.972 | 0.954 |
| $f_1/kHz$ | 5.372 | – | 0.252 | 1.477 | 3.376 | 1.036 | 17.60 |
| $R_p/\Omega\,cm^2$ | $7.6 \times 10^4$ | 301 | $5.1 \times 10^5$ | $8.6 \times 10^5$ | $3.0 \times 10^6$ | $1.6 \times 10^7$ | $7.4 \times 10^6$ |
| $C_p/nF\,cm^{-2}$ | 567 | 77600 | 216 | 98 | 63 | 25 | 18 |
| $a_p$ | 0.267 | 0.680 | 0.312 | 0.391 | 0.381 | 0.33 | 0.803 |
| $f_2/Hz$ | 3.7 | 6.77 | 1.4 | 1.6 | 0.8 | 0.4 | 1.2 |
| $R_b/\Omega\,cm^2$ | $7.3 \times 10^{15}$ | $6.2 \times 10^8$ | $5.7 \times 10^{13}$ | $1.9 \times 10^{13}$ | $2.6 \times 10^{12}$ | $4.7 \times 10^{12}$ | $1.3 \times 10^{14}$ |
| $C_b/\mu F\,cm^{-2}$ | 10.8 | 1.5 | 3.13 | 4.7 | 4.6 | 6.1 | 0.74 |
| $a_b$ | 0.906 | 0.958 | 0.893 | 0.91 | 0.872 | 0.841 | 0.875 |
| $f_3/Hz$ | $2 \times 10^{-12}$ | $1.7 \times 10^{-4}$ | $9 \times 10^{-10}$ | $1.2 \times 10^{-8}$ | $1.3 \times 10^{-8}$ | $5.5 \times 10^{-9}$ | $2 \times 10^{-4}$ |
| $\sigma$* | 1.07 | 1.8 | 3.6 | 3.9 | 2.9 | 2.8 | 1.53 |

* Coefficient $\sigma$ measures the fitting quality (maximal at $\sigma = 1$).

and ageing time, similarly to the thickness of the intermediate layer.

If the thickness of the porous layer, $d$, is assumed to be approximately 20 $\mu$m in every case, as repeatedly found with various procedures, the capacitance $C_{pw}$ calculated from the expression $C = \varepsilon_0 \varepsilon S/d$ should be about $4.4 \times 10^{-10}$ F for $S = 1\,cm^2$, a vacuum dielectric constant $\varepsilon_0 = 8.854 \times 10^{-14}\,F\,cm^{-1}$ and the permittivity of alumina ($\varepsilon = 10$) [5]. In fact, $C_{pw}$ is about twice as high on average (see Table 1); therefore, the contamination of anhydrous alumina by sulphate ions increases its permittivity by a factor of about 2, which is quite plausible.

If a permittivity of 20 for the barrier layer is also assumed, $C_b$ values about 1 $\mu$F (e.g., those calculated from the impedance diagrams and given in Table 1) would lead to a barrier layer thickness of 17.7 nm. This is consistent with the result expected from the use of an anodizing voltage of 15 V (the films thus formed are widely accepted to be 1.0–1.4 nm $V^{-1}$ thick) [3]. As can be seen from Table 1, 1000 times thicker porous layers give, approximately, 1000 times smaller $C_{pw}$ values.

Parameter $C_p$ must be the capacitance of the pore filling (Fig. 11), in parallel to the hexagonal cell walls. The overall pore cross-sectional area accounts for about 17% of the apparent surface area. As hydration develops (i.e., as the exposure time increases), $C_p$ tends to decrease to nearly the same level as $C_{pw}$ (the nF range); however, the former can be initially much higher (Table 1). Assuming that hydration has progressed to an extent where $C_p$ is one order of magnitude higher than $C_{pw}$, because the pore area will be 17% of the overall area, the permittivity of the filling must be about 50 times higher than that of anhydrous alumina contaminated with sulphate ions in cell walls; the thickness will be identical in both cases.

Because the time constant results in characteristic frequencies in the nHz range (Table 1) which are distant from the lowest frequency used in the tests (1 mHz), estimated (extrapolated) $R_b$ values will be highly uncertain. However, the data in Table 1 suggest

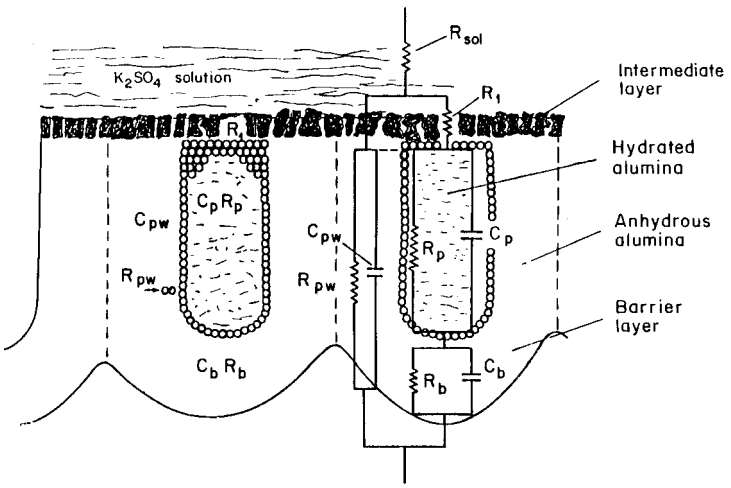


Fig. 11. Schema of the structure of an anodized aluminium oxide film. Proposed EC is superimposed.

that $R_b$ must be in the $G\Omega\,cm^2$ range or higher. If this order of magnitude and a barrier layer thickness of 20 nm are accepted, then the resistivity of the barrier layer will be $\rho_b = 1 \times 10^9\ \Omega\ cm^2/20 \times 10^{-7}\,cm = 5 \times 10^{14}\ \Omega\,cm$, which is consistent with the data for alumina in the Goodfellow catalogue [18].

By contrast, calculations based on the resistance of the porous layer, $R_p$, measurements of which from the impedance diagrams are unquestionable, lead to rather different values. Based on file SS3A in Table 1 and a porous layer thickness of 20 $\mu$m, the corresponding $R_p$ value gives $\rho_p = 3.0 \times 10^6\,\Omega\,cm^2/20 \times 10^{-4}\,cm = 1.5 \times 10^9\,\Omega\,cm$, which is roughly 5 orders of magnitude smaller than the previous $\rho_b$ value. Therefore, the pore filling is a much better conductor than the cell walls and barrier layer, whatever the extent of hydration and that of disappearance of residual intercrystalline water. A newly sealed or scarcely aged film would possess an even lower resistivity; for example, conventional sealing in boiling de-ionized water (file S45MIN in Table 1) leads to $\rho_p = 7.6 \times 10^4\,\Omega\ cm^2/20 \times 10^{-4}\,cm = 3.8 \times 10^7\,\Omega\,cm$ for the porous layer.

### 4.3. *Advantages and shortcomings of standard tests*

Anodized aluminium for industrial uses has long been assessed for adequate sealing quality in order to ensure durability and preserve the appearance of anodized materials exposed to natural environments. This has traditionally been done by using standard quality control tests such as the dye spot, 1 kHz admittance measurements and the phosphochromic acid dissolution test [2], the respective acceptance thresholds of which are level 2 (on a scale from 0 to 5) for the residual dye spot, less than 20 $\mu$S for a test surface of 133 $mm^2$ and a mass loss of 30 $mg\,dm^{-2}$.

However, standards tests, which are adequate for pass–fail controls, lack the discerning capacity required for quality levels slightly above industrial demands, as shown by the data of Table 2. In fact, the dye spot test can detect no differences among sealed specimens exposed (aged) for variable lengths of time; also, the results of the 1 kHz admittance and acid dissolution tests hardly change with time.

*Table 2. Variation of industrial seal quality indices and the resistance of the porous layer* ($R_p$) *for specimens sealed in boiling de-ionized water for 45 min with the time of atmospheric exposure*

| *Time* | *Dye spot* (*1–5*) | *Acid dissolution* /$mg\,dm^{-2}$ | *Admittance* /$\mu$S | $R_p$ /$k\Omega\,cm^2$ |
|---|---|---|---|---|
| 0 | 0 | 12.4 | 30 | 56 |
| 1 month | 0 | 13.8 | 30 | 73 |
| 3 months | 0 | 17.2 | 27 | 109 |
| 6 months | 0 | 18.1 | 20 | 113 |
| 9 months | 0 | 12.8 | 13 | 242 |
| 1 year | 0 | 16.9 | 22 | 277 |
| 2 years | 0 | 10.7 | 10 | 430 |
| 3 years | 0 | 16.1 | 10 | 820 |
| 17 years | 0 | 5.4 | 5.2 | 4500 |
| 20 years | 0 | 10.4 | 6.0 | 6400 |

This shortcoming has prompted the search for much more sensitive techniques for characterizing the physical and chemical properties of industrially anodized materials. Despite the above-mentioned lack of precision arising from gradual changes in hydration of the pore filling, the EIS technique provides much more detailed information on the characteristics of anodized films than do standard industrial seal quality control tests, as can readily be inferred by comparing the data of Table 2. In contrast with the results of the standard tests, the $R_p$ values provided by impedance tests vary over enormously wide ranges. This is also the case with other properties of anodized films such as $C_p$. As can be seen from Fig. 12, which was constructed from estimated $R_p$ and $C_p$ values in Table 1.

Although highly scattered, the $R_p$ values fit the following equation:

$$R_p(M\Omega) = 0.002 + 0.29\,t\ (\text{months}) \qquad (3)$$

This equation is graphically represented by the solid line in Fig. 12. Apparently, pore resistance increases by about 0.29 $M\Omega\,month^{-1}$.

After pores are filled by a reacting solution, the complex sealing and ageing mechanisms that follow involve successive gelling, thorough plugging of pores by the condensed gel, crystallization, agglomeration and ageing for years or even decades [8], with the gradual, very slow disappearance of intercrystalline water. These transformations in the pore filling increase the resistivity of the porous layer and proportionally increase $R_p$ as the material concerned ages. These changes cause a simultaneous decrease in the filling permittivity, $\varepsilon$; that is, in the capacitance of the porous layer ($C = \varepsilon_0 \varepsilon S/d$), as can be seen from Fig. 12, which reflects diametrically opposed trends for $R_p$ and $C_p$.

As a result, the impedance at a given frequency can be used for the highly accurate estimation of the electrochemical parameter for oxide films represented by each component of the EC. These parameters, in turn, can thus be used to analyse the effects on any factor in the sealing and ageing of anodized aluminium oxide films, and on their physicochemical properties.

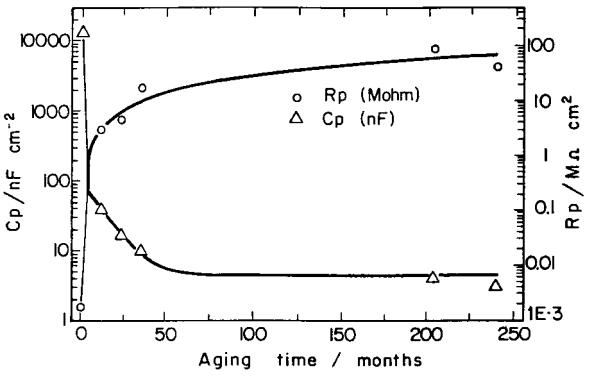


Fig. 12. Variation of $R_p$ (○) and $C_p$ (△) with ageing time. Solid line corresponds to data fitted to Equation 3.

## 5. Conclusions

The results allow the following conclusions:

(i) The EIS technique is much more sensitive than standard seal quality control tests.
(ii) It reveals that ageing of anodized films develops for years, or even decades; by contrast, standard control tests lose their discriminating ability at quality levels slightly above current industrial demands.
(iii) In addition to assessing sealing quality, EIS allows information of transformations occurring throughout the thickness of anodized films to be obtained, as well as on the electrical properties of such films, the integrity of the barrier and porous layer, and on the effect of any factor potentially influencing sealing and ageing of the film.

## Acknowledgements

This work was supported by *Comisión Interministerial de Ciencia y Tecnología* (CICYT) of the Ministry of Education and Culture of Spain (Project MAT95-0060).

## References

[1] A. W. Brace, 'The Technology of Anodizing Aluminium' (Tecnicopy Ltd, Stonenhouse, Gloucesterhire, (GB), 1979 pp. 1–19.
[2] Anon, *Standards ISO 2143* and *2931*.
[3] T. P. Hoar and G. C. Wood, *Electrochim. Acta* **7** (1962) 333.
[4] J. Hitzig, K. Juttner, W. J. Lorenz and W. Paatsch, *J. Electrochem. Soc.* **103** (1986) 887.
[5] J. Hitzig, K. Juttner, W. J. Lorenz and W. Paatsch, *Corros. Sci.* **24** (1984) 945.
[6] F. Mansfeld, *Corrosion, NACE* **44** (1988) 856.
[7] B. van der Linden, H. Terryn and J. Vereecken, *J. Appl. Electrochem.* **20** (1990) 798.
[8] R. Lizarbe, J. A. González, E. Otero and V. López, *Aluminium* **69** (1993) 548.
[9] R. Lizarbe, V. López y J. A. González, *Pinturas y Acabados Industriales* **35**(207) (1993) 70.
[10] R. Lizarbe, W. López, E. Otero y J. A. González, *Rev. Metal, Madrid* **26** (1990) 359.
[11] N. Celati, M. C. Sainte Catherine, M. Keddam and H. Takenouti, *Mater. Sci. Forum* **192** (1995) 335.
[12] G. C. Wood, *Trans. Inst. Metal Finish.* **36** (1959) 220.
[13] K. Wefers, *Aluminium*, **49** (1973) 553, 622.
[14] K. Shimizu, K. Kobayashi, G. E. Thompson and G. C. Wood, *J. Appl. Electrochem.* **15** (1985) 781.
[15] G. E. Thompson, R. C. Furneaux and G. C. Wood, *Corros. Sci.* **18** (1978) 481.
[16] G. E. Thompson and G. C. Wood, *Nature* **290** (1981) 230.
[17] C. M. Abreu, M. Izquierdo, M. Keddam, X. R. Nóvoa and H. Takenouti, *Electrochim. Acta* **41**(15) (1996) 2405.
[18] 'Goodfellow Catalogue'. Ed. Goodfellow, Cambridge Science Park (England) (1996/7), p. 409.